JCTC Journal of Chemical Theory and Computation

Catalytic Reaction Mechanism of Oxalate Oxidase (Germin). A Hybrid DFT Study

Tomasz Borowski,*,† Arianna Bassan,† Nigel G. J. Richards,# and Per E. M. Siegbahn†

Department of Physics, Stockholm Center for Physics, Astronomy and Biotechnology, Stockholm University, S-106 91, Stockholm, Sweden, and Department of Chemistry, University of Florida, Gainesville, Florida 32611-7200

Received February 25, 2005

Abstract: The mechanism of the catalytic reaction for oxalate oxidase has been investigated with the hybrid density functional method B3LYP. The models used in the calculations comprise of the manganese ion, three imidazoles, and one acetate, which model the active-site Mn(II) and its first-shell protein ligands. Moreover, the reactants, i.e., singly protonated oxalate and dioxygen, have been explicitly considered. The computational results suggest that the enzyme−oxalate complex can adopt two conformations, one with bidentate oxalate and 6-coordinate manganese and the second one with monodentate substrate and coordinatively unsaturated Mn(II). This second species reacts with dioxygen on the quartet potential energy surface, and in a rate-limiting step yields one CO_2 molecule and a reactive intermediate, in which Mn(III) is coordinated by HOO^- and a formyl radical anion. A subsequent fast spin transition, from the quartet to the sextet spin state, allows an electron transfer from the formyl radical anion to Mn(III) and leads to the product−enzyme complexes. It is proposed that the final step of the catalytic cycle involves protonation of these species and release of products. Taken together, the mechanistic proposal presented in this work agrees well with the available experimental data and provides an explanation for the very efficient coupling between the two-electron dioxygen reduction and oxalate oxidation performed by oxalate oxidase.

I. Introduction

Oxalate oxidase, also known as germin, hereafter abbreviated as Oxo, is a protein germination marker usually found in the cereals embryos. Although its role in plant development is still not fully understood, the Oxo catalyzed degradation of oxalate (Scheme 1) releases H_2O_2 which is needed for cross-linking in cell wall and may also promote tissue remodeling.[1] Moreover, some pathogens utilize oxalic acid to reduce pH and in this way stimulate polysaccharolytic enzymes, which digest the plant tissues. For this reason, transgenic crops with elevated Oxo expression are less prone to infection due to their efficiency in oxalic acid decomposition. Finally, Oxo is used as an analytical enzyme in procedures for determination of oxalic acid levels. The reader interested in the broader picture of oxalate metabolism and its enzymology is referred to the currently published review.[2]

Scheme 1: Oxo Catalytic Reaction

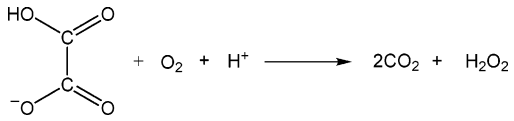

Biochemical studies showed that Oxo is a homohexameric enzyme binding one manganese ion per subunit.[3,4] Since neither flavins nor other transition metals are required for the catalysis, it was proposed that Mn(II) plays an active role in the enzymatic mechanism.[4,5] Barley Oxo shows maximum activity at pH 3.8, which falls between the two pK_a values for oxalic acid, namely 1.2 and 4.1. This, in turn, indirectly indicates that the singly protonated form of oxalate is the reactive species binding to Oxo.[5,6] Further important

* Corresponding author phone: +46 8 55378703; fax: +46 8 55378601; e-mail: borowski@physto.se.
† Stockholm University.
# University of Florida.

10.1021/ct050041r CCC: $30.25
Published on Web 04/29/2005

Scheme 2: Experiment Suggested Mechanisms for the Oxo Catalytic Reaction

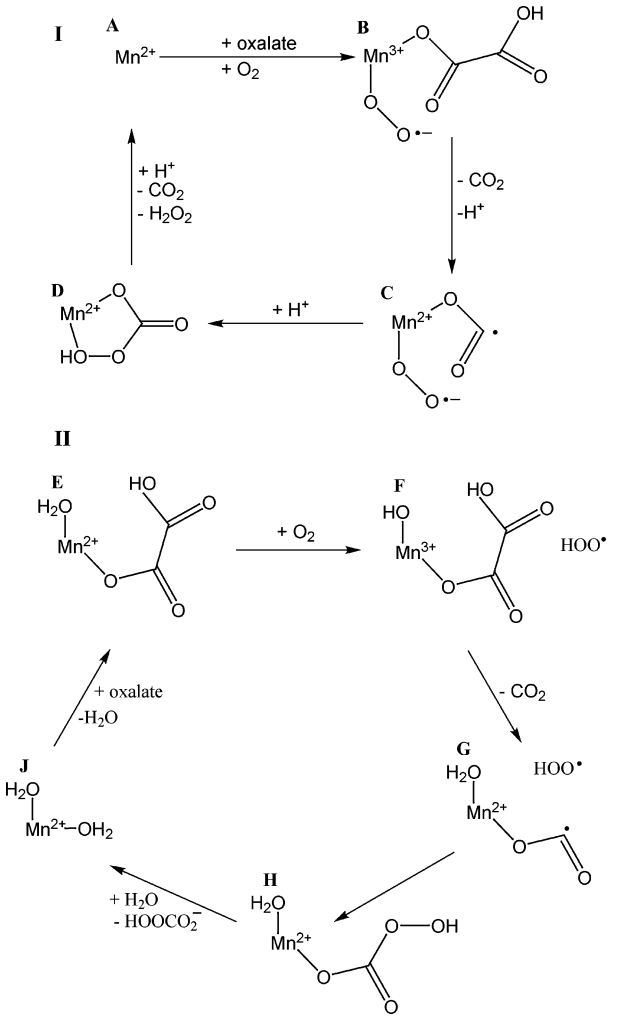

data concerning the reaction mechanism were provided by EPR measurements done both for the native enzyme and under turnover conditions.[6] Notably, it was shown that the native form of Oxo binds high-spin Mn(II) in roughly octahedral environment and that this site is not perturbed in the presence of H_2O_2, which is one of the catalytic reaction products. However, addition of oxalate alters the EPR signal, which indicates that the substrate directly coordinates Mn(II). Like for the native form, the EPR spectrum for this enzyme−substrate complex was found to be consistent with the six-coordinate Mn(II) site. Importantly, the measurements under turnover conditions showed that no free radicals are released into solution, which inevitably implies a tight coupling between dioxygen reduction and oxalate oxidation. In the same study[6] it was found that a minor fraction of the isolated enzyme (ca. 5%) binds high-spin Mn(III) ion in a distorted octahedral environment. Under anaerobic conditions this species reacts with oxalate producing Mn(II) and carboxylate radicals, which demonstrates that the Mn(III) form of the Oxo active site is capable of oxalate oxidation. However, the EPR study under turnover conditions ruled out the possibility that this Mn(III) form of Oxo is catalytically competent. Taken together, the experimental data led to the mechanistic proposals shown in Scheme 2.

In the first step of the mechanism proposed by Bornemann et al. (I in Scheme 2), oxalate binds to Mn(II) in the active site of Oxo and, through lowering the metal red-ox potential, activates it for binding of dioxygen.[4,7] In the reactive ternary Oxo−Mn−oxalate−O_2 complex (**B** in Scheme 2) manganese ion is one-electron oxidized by dioxygen which acquires superoxide character. Subsequent release of the first CO_2 molecule leads to the Oxo−Mn(II)−superoxide−formyl radical complex (**C**), which collapses to the Oxo−Mn(II)−peroxocarbonate complex (**D**). The protonation of **D** leads to its decomposition to H_2O_2 and the second CO_2 molecule. This mechanistic proposal satisfies the requirement of a tight coupling between dioxygen reduction and oxalate oxidation, which guarantees that no radicals escape from the enzyme active site. In addition, assuming that the reactive complex **B** is short-lived, only the Mn(II) species would be detectable, which agrees with the EPR data.[6] The alternative mechanism was proposed by Whittaker and Whittaker, and it is shown in Scheme 2 II.[6] In this case, oxalate is supposed to bind to Mn(II) in a monodentate fashion, and one water molecule remains bound to manganese (**E**). The hydrogen atom transfer from Oxo−Mn(II)−oxalate−OH_2 to externally bound dioxygen gives essentially free hydroperoxide radical and the Oxo−Mn(III)−oxalate−OH complex (**F**). The proton-coupled electron transfer (PCET) within the latter species affords a biradical intermediate **G**, which collapses forming the product complex **H**. The last step is a simple replacement of the peroxocarbonate by a water molecule, which produces the native form of Oxo (**J**).

The 1.6 Å-resolution crystal structure of the native Oxo revealed that Oxo is a homohexamer with the fold characteristic for the cupin superfamily.[8,9] The active site manganese is bound to three histidines (His88, His90, and His137) and one glutamate (Glu95) protein side chains, while the remaining two sites in the coordination octahedron are occupied by water molecules.[8] The structure of the barley Oxo−Mn−oxalate complex is currently not known; however, the putative oxalate decarboxylase (TM1287) from *Thermotoga maritima* was recently cocrystallized with oxalate.[10] Remarkably, in this structure a metal ion has an octahedral coordination with oxalate bound in a bidentate fashion, though the identity of the metal is currently not known. The other ligands are the same as in the barley Oxo (three His and one Glu).

The catalytic rate constant (k_{cat}) of barley Oxo was measured to be 22 s^{-1}, which corresponds to the activation barrier $\Delta G^{\ddagger}$ of 15.6 kcal/mol (at 298 K).[5]

In summary, the experimental data led to the formulation of two hypothetical mechanisms for the Oxo catalytic cycle. Detailed understanding of the chemical steps involved in the reaction is, however, still missing. For example, the point at which the necessary spin-crossing occurs is not known, as is the character of the reactive intermediates formed along the reaction coordinate. In this work hybrid density functional theory (DFT) has been used to study the mechanism of the Oxo catalytic cycle. The results reported here, when combined with known experimental data, lead to a detailed description of the catalytic reaction of Oxo and provide new insight into the Mn/oxalate chemistry.

Scheme 3: Suggested Mechanism for the Oxo Catalytic Reaction

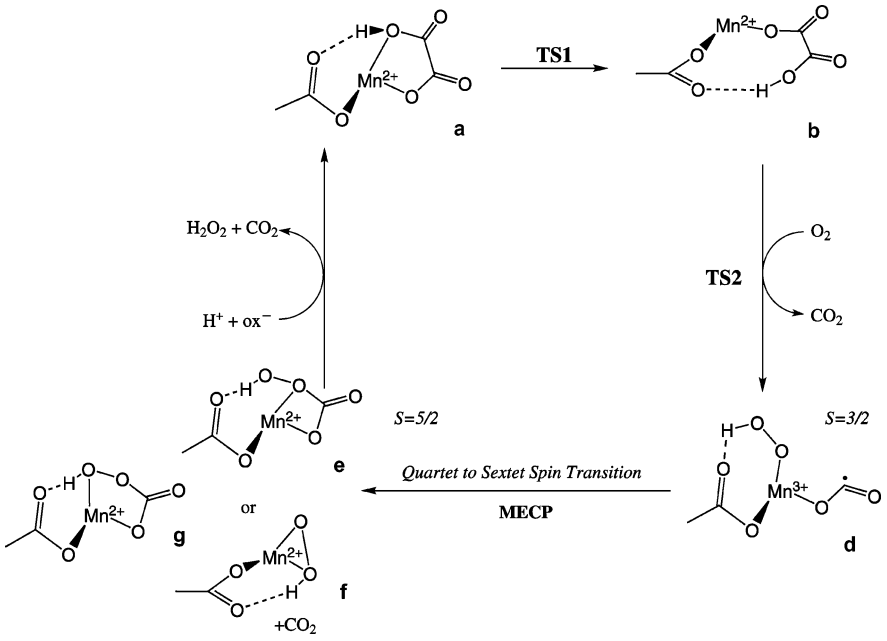

II. Computational Details

The model of the Oxo active site is based on the crystal structure solved for the native protein (PDB code: 1Fl2). Since the amino acids from manganese second coordination shell (Asn, Gln, Phe, Val, and Met) are unlikely to play an active role in catalysis, only the manganese first-shell ligands (His88, His90, His137, and Glu95) are included in the computational model. Histidines are modeled with imidazoles, while glutamate is replaced by acetate. The positions of the hydrogens introduced in place of the omitted parts of histidines are constrained throughout the calculations. For acetate, the position of the methyl carbon is constrained. In this way, the rigidity of the protein matrix is taken into account in an approximate way. Two water molecules coordinating Mn(II) in the native form of the enzyme have been substituted with singly protonated oxalate. The motivation for this charge state of the substrate comes from the biochemical data. Namely, Oxo exhibits maximum activity for pH between the two pK_a values for oxalic acid, which means that the singly protonated oxalate is the dominating form of the substrate under the optimum pH conditions.[5,6]

All calculations have been performed employing hybrid DFT with the B3LYP exchange-correlation functional.[11,12] Two programs, Gaussian03[13] and Jaguar,[14] have been used. Geometry optimizations have been done with a valence double-ζ basis set coupled with an effective core potential describing the innermost electrons on manganese. This particular basis set is labeled lacvp in Jaguar. For the optimized structures the electronic energy has been computed with a bigger basis set of triple-ζ quality with polarization functions on all atoms (labeled lacv3p** in Jaguar). The solvent corrections have been calculated with the self-consistent reaction field method implemented in Jaguar.[15,16] A dielectric constant of 4 with a probe radius of 2.50 Å have been used to model the protein surrounding of the active site.

The structure of the minimum energy crossing point (**MECP**) between noninteracting quartet and sextet states has been located at the B3LYP/lacvp level of theory employing the methodology developed by Harvey et al.[17] Since in this computational procedure it is not possible to use constraints, these calculations have been performed without frozen coordinates, i.e., the activation energy for reaching the **MECP** geometry is computed from the energy of an unconstrained model of intermediate **d** (see Scheme 3).

For the optimized geometry of the quartet−sextet **MECP** the coupling between the two states due to the spin−orbit coupling (SOC) operator has been estimated in the following way. First, the model has been truncated to afford CASSCF calculations. With this respect, the imidazole ligands have been replaced with ammonia molecules and acetate with formate. This model has subsequently been used for spin−orbit coupling calculations, which have been accomplished with the GAMESS program.[18] The wave function of the sextet state has been optimized at the ROHF/6-31G(d) level, and subsequently the quartet wave function has been converged at the CASSCF(5,5) level keeping the core orbitals frozen from the sextet state. The effective one-electron operator approximation has been assumed for the SOC, and the recommended effective nuclear charges have been employed.[19,20] The quartet−sextet transition probability (P) has been estimated from the Landau−Zener formula[21]

$$P = 1 - e^{-2\delta} \tag{1}$$

where

$$\delta = \frac{\pi |H_{ij}|^2}{\hbar \nu |\Delta g_{ij}|} \tag{2}$$

and where H_{ij} is the spin−orbit coupling matrix element between the two electronic states, ν is the velocity with which the system is passing the crossing region, and Δg_{ij} is the difference of the gradients calculated for the two states at

the crossing point. These gradients have been evaluated by numerical differentiation of the energy with respect to a small geometrical (5 degrees) displacement along the approximate spin-transition reaction coordinate, which is the O−C−O angle in the formyl radical anion in species **d**.

Since in several intermediates found in this study the spins on various parts of the complexes are antiferromagnetically coupled, a spin correction to the energy of these species has been calculated using the broken symmetry approach.[22,23] The recommended strong localized limit has been assumed, which means a zero overlap between the magnetic orbitals.[23] This specific computational methodology has successfully been applied to a wide range of redox enzymes with transition metals at their active sites.[24−26]

Finally, a short comment on the energies reported in this work. The reported values are the electronic energies calculated at the B3LYP/lacv3p**//B3LYP/lacvp level of theory plus the solvent effect calculated at the B3LYP/lacvp level. Zero energy corresponds to the isolated reactants, i.e., the Oxo-(singly protonated)oxalate complex and dioxygen. Thus, neither thermal corrections to the energy nor the entropic term are taken into account. However, while the former is usually on the order of a few kcal/mol, the entropy term is significant for the steps where small molecules are either trapped or released. For example, at room temperature the entropy term may contribute up to 10 kcal/mol to the free energy of the reaction in which dioxygen is bound to the model of the metal-containing active site. Therefore, due to this entropic term and to a lesser extent due to the thermal corrections to enthalpy, the true free energy profile will deviate from the one calculated here. However, the main goal of this study is to find the most likely mechanism of Oxo catalytic cycle by testing various a priori plausible mechanisms. For this purpose a semiquantitative description of the free-energy profile along the reaction coordinate seems sufficient because the thermal and entropy corrections are supposedly rather similar for the mechanisms tested in this work. The more quantitative description of the free-energy profile will be based of the QM/MM study which is now in progress.

III. Results and Discussion

Within this work several a priori plausible mechanisms have been tested, but only one involves a reasonable activation barrier, and this mechanism is presented below. The discarded mechanisms involve significantly higher barriers, and they are shortly summarized at the end of the manuscript and in the Supporting Information. The suggested mechanism is shown in Scheme 3, while the elementary steps of which it consists are discussed in detail in the following subsections.

Oxalate Coordination. The EPR data reported for the Oxo−Mn(II)−oxalate complex is indicative of a six-coordinate manganese in the active site, though binding of the substrate markedly changes the spectrum with respect to that for the native enzyme. Therefore, a direct interaction between Mn(II) and oxalate was proposed.[6] Moreover, the crystal structure of TM1287[10] shows a bidentate oxalate, which might suggest a similar binding mode in the Oxo−Mn(II)−oxalate complex. However, such an arrangement

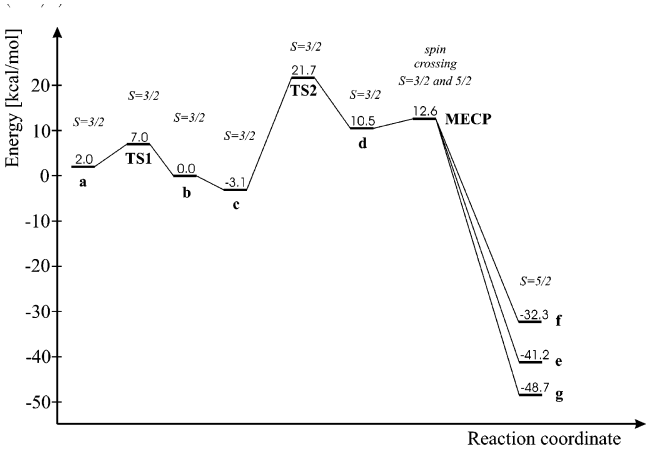

Figure 1. The calculated energy profile along the suggested reaction path for the Oxo catalytic cycle. The reported spin quantum number for **a**, **TS1**, and **b** takes into account the spin of unbound dioxygen (*S*=1) antiferromagnetically coupled with the spin on Mn(II) (*S*=5/*2*).

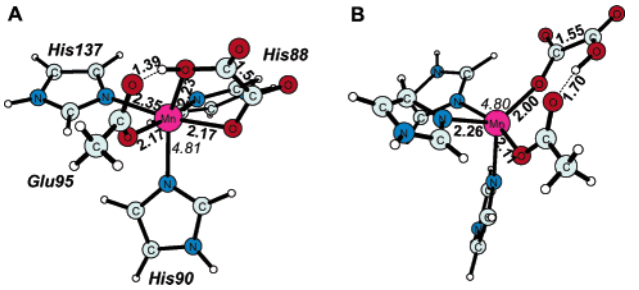

Figure 2. Optimized structures for the two forms of the Oxo−Mn(II)−oxalate complex (*S*=5/2). A. The six-coordinate form **a** and B. the five-coordinate form **b**. Distances in bold, spin populations in italics.

results in a six-coordinate Mn(II) ion, which lacks any vacant site available for dioxygen binding and, therefore, implicates either that dioxygen does not bind to Mn during the reaction or that the coordination number of manganese changes from 6 to 5 before O_2 binding. As shown below, the latter alternative is supported by the calculations.

The Oxo−Mn(II)−oxalate complex is calculated to exist as a nearly unimolar mixture of two species, one with bidentate oxalate (**a** in Scheme 3) and the second, **b**, with a five-coordinate Mn(II) and monodentate substrate. The energy difference between the two species is only 2 kcal/mol (see Figure 1). In the six-coordinate species (**a**), the protonated carboxylic group of the substrate both coordinates Mn(II) and forms a hydrogen bond with Glu95 (see Figure 2A). In the case of the five-coordinate form **b**, the protonated carboxylic group of the substrate is rotated away from manganese so that only the hydrogen bond between this group and Glu95 is preserved.

The transformation of **a** into **b** is favorable by 2 kcal/mol. Since this species is not the one observed experimentally, this indicates a small error in the calculations. However, the energy difference between **a** and **b** is quite small and therefore could change sign if the second shell ligands were taken into account. Indeed, preliminary QM/MM calculations performed for the extended model of the Oxo active site favor

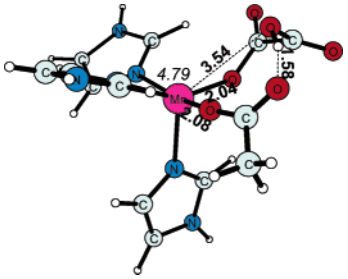

Figure 3. Optimized structure of **TS1** – the transition state which connects the two forms of the Oxo−Mn(II)−oxalate complex (*S*=5/2). Distances in bold, spin populations in italics.

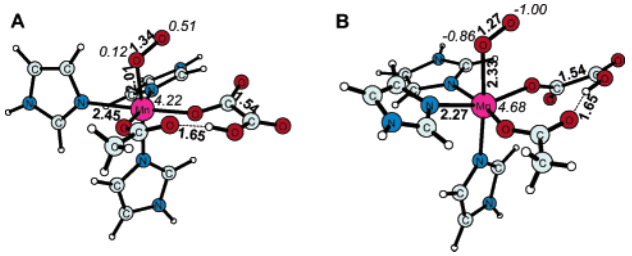

Figure 4. Optimized structures for Oxo−Mn−oxalate−O_2 complexes. A. The sextet species (*S*=5/2) and B. the quartet complex **c** (*S*=3/2). Distances in bold, spin populations in italics.

the six-coordinate species and thus agree well with the EPR data.[6] The transformation of **a** into **b** is a relatively simple geometrical rearrangement and involves a rather low activation barrier of 5 kcal/mol (for the transition state geometry see Figure 3).

Dioxygen Binding. The five-coordinate Oxo−Mn(II) species **b** possesses a vacant position at which dioxygen can bind. Due to the open-shell electronic structure of both high-spin Mn(II) and dioxygen, three possible spin states can be envisaged for the Oxo−Mn−dioxygen complex: octet (S=7/2), sextet (S=5/2), and quartet (S=3/2). In the octet state all of the unpaired electrons of the reactants are ferromagnetically coupled, which leads to no net bonding between dioxygen and manganese. In the optimized octet structure the Mn−dioxygen distance is large (3.3 Å), which together with the spin populations, 4.8 on Mn and 2.0 on dioxygen, clearly indicates that dioxygen does not bind to manganese in the octet spin state.

Flipping one spin in the octet electronic configuration leads to the sextet state, which is best described as a complex between high-spin Mn(III) and a superoxide anion. Indeed, the spin populations (4.2 on Mn and 0.63 on dioxygen) and the O−O bond distance in the dioxygen ligand (1.34 Å, see Figure 4A) support this interpretation. This state is computed to lie quite high in energy, 12.1 kcal/mol above the energy of the separated reactants in their electronic ground state. Even though this energy is not prohibitively high, all attempts to find a feasible reaction mechanism involving this sextet Oxo−Mn−oxalate−O_2 species failed, since in all cases the transition states turned out to have too large barriers (vide infra).

Finally, the antiferromagnetic coupling of spins on manganese and dioxygen leads to the Oxo−Mn−oxalate−O_2 in the quartet state (see Figure 4B). In this case, dioxygen forms

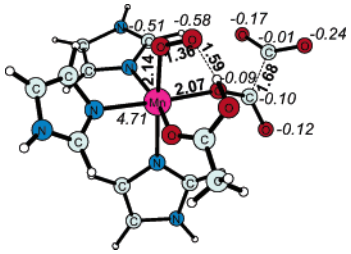

Figure 5. Optimized structure of the transition state (**TS2**) for the initial one-electron oxidation of oxalate (*S*=3/2). Distances in bold, spin populations in italics.

a weak bond to manganese (2.33 Å), while the spin populations indicate that dioxygen preserves its triplet character and Mn remains divalent. The calculated complexation energy is negative, i.e. −3.1 kcal/mol with the broken-symmetry correction, though, too small to compensate for the entropy loss caused by dioxygen trapping (around 8−10 kcal/mol). Therefore, it is concluded that dioxygen does not make any stable complex with the Oxo active site but only short-lived adducts which either react further or decompose back into the reactants. With respect to this instability of the dioxygen-bound species, it is important to notice the difference between the sextet and quartet spin states. Not only is the quartet state far more stable than the sextet counterpart (by 15.2 kcal/mol), but it is also directly accessible on the ground state potential energy surface (PES) of the reactants. In other words, the quartet species directly dissociates to the reactants in their ground state, while for the sextet state a spin transition must first take place before the dissociation.

Reduction of Dioxygen. The second step of the Oxo catalytic reaction is best described as a proton coupled electron transfer (PCET) from oxalate to dioxygen. However, this description is further complicated by the fact that, concomitantly with the proton and the first electron, a second electron, formally from Mn(II), is transferred to the dioxygen ligand. Thus, this step can be viewed as PCET coupled with another electron transfer (ET), since in this reaction dioxygen is reduced to the Mn-bound hydroperoxo anion, oxalate is one-electron oxidized to a formyl radical anion and CO_2, while Mn(II) is oxidized to Mn(III). The optimized structure of the transition state (**TS2**) for this process is presented in Figure 5. Notably, the proton involved in the PCET, originally from oxalate, is bound to Glu95 and positioned appropriately to form a hydrogen bond to the dioxygen ligand. Moreover, two bonds are significantly elongated with respect to the quartet Oxo−Mn−oxalate−O_2 complex (Figure 4B). First, the O−O bond distance in the dioxygen ligand increases from 1.27 to 1.36 Å, and this elongation is accompanied by a decrease of the O_2 spin population from −1.86 to −1.09. Second, the C−C bond of oxalate is elongated from 1.54 to 1.68 Å at the same time as the gross spin population on the oxalate ligand increases from 0.05 to −0.73. The spin on Mn does not change much when going from **c** to **TS2** (from 4.68 to 4.71), which suggests that the second electron 'lags behind'. The normal mode with imaginary frequency, which corresponds to the reaction coordinate, involves the elongation of the C−C bond in

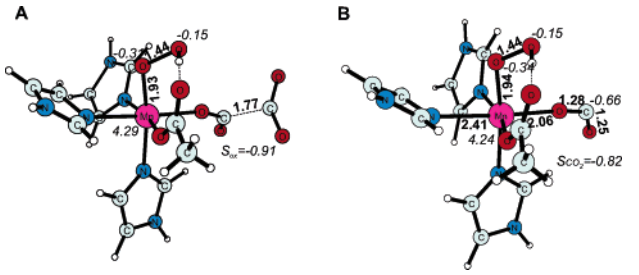

Figure 6. Optimized structures of the products of the initial one-electron oxidation of oxalate. A. The metastable species with oxalate radical anion (*S*=3/2) and B. the stable complex **d** with formyl radical anion (*S*=3/2). Distances in bold, spin populations in italics, ox stands for oxalate.

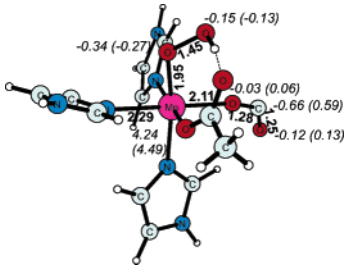

Figure 7. Optimized structure of the quartet−sextet minimum energy crossing point (**MECP**; *S*=3/2 and 5/2). Distances in bold, spin populations in italics, in parentheses spin populations for the sextet state.

oxalate and the protonated Glu95 approaching the distal O_2 oxygen atom, both movements in phase. Considering the energetics, the calculated activation energy is quite high, i.e., 21.7 kcal/mol, which is 6.1 kcal/mol more than the barrier estimated from the experimentally determined k_{cat} value (15.6 kcal/mol). Since all other investigated mechanisms involve substantially higher barriers, it is believed that the error of 6 kcal/mol is acceptable, and the suggested mechanism is the one used by Oxo.

Once the reacting system traverses **TS2**, the second electron is transferred from Mn(II) to the dioxygen ligand, and the species with a hydroperoxo anion coordinated to Mn(III) is formed. In the optimized complex (Figure 6A), the one-electron oxidized oxalate forms an oxalate radical anion with a carbon−carbon distance of 1.77 Å and a gross spin population of −0.91. However, this species is not stable with respect to the elongation of the C−C bond in the oxalate ligand. More specifically, when this distance is gradually elongated, first the energy remains approximately constant, but at a larger interatomic separation it slowly decreases. Therefore, the computational results indicate that once the **TS2** is passed, the first CO_2 molecule is liberated, while the active site Mn(III) ion binds HOO^- and $CO_2^{\bullet-}$, i.e., intermediate **d** (Figure 6B) is formed. Interestingly, the species **d** is a Jahn−Teller Mn(III) system with a weak J−T axis in the direction of the Mn-formyl radical anion bond. From Figures 4B and 6B it can be noticed that the Mn−His137 distance increases from 2.27 to 2.41 Å when going from **c** to **d**.

Spin-Crossing. In the intermediate **d**, formed in the one-electron oxidation of oxalate, the spins on the Mn(III) ion and the formyl radical anion are antiferromagnetically coupled (see Figure 6B). Such an electronic configuration is responsible for the stability of this species, since the electron transfer to Mn(III) would lead to an excited electronic configuration of manganese center (four d electrons with alpha spins, one with beta). If the electrons had parallel spins, which is the case in the sextet spin state, the electron transfer would be straightforward and would lead to the products in their ground state. For these reasons, the activation barrier connected with the quartet to sextet spin transition has been calculated by finding the minimum energy crossing point (**MECP**) where the two potential energy surfaces cross. The optimized geometry of the **MECP** is shown in Figure 7. Considering the electronic structure, the reported spin populations for the quartet and sextet states show that the spin transition can be viewed as a spin flip of the electron localized mostly on the carbon atom of the formyl radical anion fragment. With respect to the geometrical structure, a comparison of the reported bond lengths with those of intermediate **d** (Figure 6B) shows that the crossing point geometry is very similar to that of the quartet species. The bond lengths in the formyl radical fragment are unchanged, while the O−C−O angle opens slightly from 132.6 to 134.6 degrees.

This very small difference between the **d** and **MECP** geometries has the consequence that the energy gap between them is also very small, i.e., 2.1 kcal/mol (see Figure 1). Thus, provided that the coupling between the two spin states is sufficiently strong, the quartet to sextet spin transition will be very fast. The estimated value of the $< quartet|H_{SO}|\ sextet >$ matrix element is 2.16 cm^{-1}, which is sufficient to produce an effective spin junction in the current system. The quartet and sextet energy surfaces are relatively flat at the **MECP** geometry, $|\Delta g_{ij}| = 12.6$ kcal/mol/rad, which combined with the H_{SO} value and the estimated speed at which the system crosses the **MECP** (1.5×10^9 rad/s; calculated assuming the 500 cm^{-1} frequency and 0.01 rad amplitude for the O−C−O bending mode) gives a crossing probability of 0.58. Taking this value as a preexponential factor leads to the apparent barrier for the spin transition of 2.5 kcal/mol. Notably, even if the crossing probability were 1 order of magnitude smaller, still the apparent barrier would be only 3.9 kcal/mol. Thus, the quartet to sextet spin transition is calculated to be very efficient, which guarantees the quantitative coupling between dioxygen reduction and oxalate oxidation.

Interestingly, the observation that the crossing surfaces are almost parallel (small $|\Delta g_{ij}|$) was also made for the reaction between dioxygen and heme proteins, and this condition was proposed to facilitate the spin transition.[27] Moreover, the fact that MECPs very often lie rather close to the minimum of the higher energy state was also noticed in previous studies.[28,29]

Finally, if oxalate decarboxylase (OxDC), an enzyme closely related to Oxo and catalyzing the breakdown of oxalate to CO_2 and formate, uses a similar mechanism for producing a formyl radical, the manganese second sphere ligands of OxDC must ensure that the protonation of the formyl radical is faster than the quartet to sextet spin transition. We are currently investigating this mechanism,

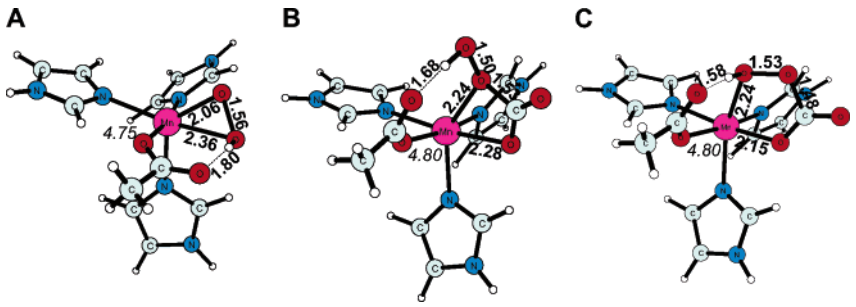

Figure 8. Optimized structures of the product complexes (S=5/2). A. The complex **f** with bidentate hydroperoxide anion, and B. and C. show species **e** and **g** with peroxocarbonate anion. Distances in bold, spin populations in italics.

and the detailed discussion of the means by which OxDC obtains its product specificity will be presented in a forthcoming paper.

Products. The spin transition discussed in the previous section enables a spontaneous electron transfer between the formyl radical anion and Mn(III). Three different products of this ET reaction have been identified. First, the CO_2 molecule formed in this ET reaction can stay in the active site and react (without any barrier) with the hydroperoxo anion. This leads to structure **e** or **g** (Figure 8B and C) with a peroxocarbonate anion chelating Mn(II). Alternatively, the CO_2 molecule can leave the active site, in which case, the hydroperoxo anion forms a second coordination bond with Mn (**f**, see Figure 8A).

The species **g**, which involves a five-member ring formed by peroxocarbonate and manganese, is the most stable form of the product complex. Interestingly, the mode of peroxocarbonate binding to the metal is similar to that observed for an iron synthetic complex.[30]

Protonation of either of these product complexes and subsequent release of H_2O_2 and CO_2 is most probably the final step of the catalytic cycle. The energetics of these steps, however, cannot be reliably calculated with the present models.

Alternative Mechanisms. Several other mechanisms of the catalytic reaction of Oxo have been tested within this study. The scheme presenting them can be found in the Supporting Information, and here only a brief description is given. In the mechanism II shown in Scheme 2 the first step is a hydrogen atom transfer from Oxo−Mn(II)−H_2O to dioxygen. The calculated energy of this reaction is 26.8 kcal/mol, and the barrier is most probably by a few kcal/mol higher. Another investigated mechanism involves the PCET on the sextet PES. This mechanism is similar to that suggested in this work, but in this case the spin transition takes place for the Oxo−Mn−O_2 complex. The calculated barrier for this mechanism is 26.2 kcal/mol. If Glu95 does not mediate the proton transfer, then a direct hydrogen atom transfer from oxalate to Mn-bound dioxygen can occur. The calculated barriers for this mechanism are 28.7 and 29.7 kcal/mol for the quartet and sextet spin states, respectively. The mechanism with an attack of Mn-bound dioxygen on the carboxylate carbon of oxalate parallels the oxidative decarboxylation reaction of α-keto acid dependent dioxygenases.[29,31−33] However, the carboxylic functional group is much less reactive than the carbonyl one. The calculated energies of the tetrahedral intermediate afforded by an attack of dioxygen/superoxide on the oxalate carbon are very high, i.e., 41.8 and 43.4 kcal/mol for the quartet and sextet PES, respectively. Finally, two mechanisms involving dissociation of one histidine ligand from manganese have been considered. In both cases oxalate chelates manganese and the liberated histidine hydrogen bonds to the HOO fragment. In the first mechanism the HOO• radical attacks oxalate, while in the second an electron is transferred from oxalate to Mn(IV). The calculated barriers connected with these mechanisms are 36.1 and 27.2 kcal/mol, respectively. In conclusion, all tested alternative mechanisms involve barriers markedly higher than that calculated for the suggested mechanism (Scheme 3). It is believed that this observation lends additional credence to the mechanistic proposal advocated in this work.

Conclusions

The results of the theoretical investigations reported here together with the published experimental data has allowed us to propose a detailed mechanism of the catalytic cycle of Oxo (see Scheme 3 and Figure 1). In summary, the Oxo−Mn(II)−oxalate complex exists as a mixture of five- and six-coordinate species. The form with coordinatively unsaturated Mn(II) site reacts with dioxygen on the quartet potential energy surface. In this step, the proton from oxalate monoanion is transferred to dioxygen through the first-shell glutamate. The proton-transfer triggers the C−C bond cleavage, and the electron follows the proton. Simultaneously, the second electron, necessary to produce the peroxo species, is provided by manganese. This step, which is also rate-limiting, yields the first CO_2 molecule and the reactive intermediate (**d**) in which the formyl radical anion coordinates the high-spin Mn(III). The quartet to sextet spin transition, which involves a small apparent barrier (ca. 2−4 kcal/mol), allows for the formyl radical → Mn(III) electron transfer. This step leads to the product−active site complex, which upon protonation decays to H_2O_2, CO_2, and the active site is then ready to begin the next catalytic cycle. Notably, the proposed mechanism satisfies the experimentally derived requirement of a tight coupling between oxalate oxidation and dioxygen reduction. Specifically, the radical intermediate **d** is predicted to be very short-lived, which guarantees the observed product specificity and no radical escape. In conclusion, the catalytic role of manganese involves the following: (i) bringing the substrates together, (ii) providing temporarily one electron necessary for dioxygen reduction, and (iii) facilitating the spin transition through an efficient spin−orbit coupling route.

The interplay of these three functions allows Oxo to perform the red-ox chemistry in an efficient and very controlled manner.

Acknowledgment. We are grateful to Sven de Marothy for providing us with his XYZ-Viewer program which was used to produce the molecular graphics presented in this manuscript. T.B. acknowledges the support from the Polish State Committee for Scientific Research (Grant 2 P04A 042 26).

Supporting Information Available: Investigated and discarded mechanism for the catalytic reaction of oxalate oxidase (Scheme S1). This material is available free of charge via the Internet at http://pubs.acs.org.

References

(1) Lane, B.; Dunwell, J.; Ray, J.; Schmitt, M.; Cuming, A. *J. Biol. Chem.* **1993**, *268*, 12239−12242.

(2) Svedruzic, D.; Jonsson, S.; Toyota, C. G.; Reinhardt, L. A.; Ricagno, S.; Lindqvist, Y.; Richards, N. G. J. *Arch. Biochem. Biophys.* **2005**, *433*, 176−192.

(3) Woo, E.-J.; Dunwell, J. M.; Goodenough, P. W.; Pickersgill, R. W. *FEBS Lett.* **1998**, *437*, 87−90.

(4) Requena, L.; Bornemann, S. *Biochem. J.* **1999**, *343 Pt 1*, 185−190.

(5) Kotsira, V.; Clonis, Y. *Arch. Biochem. Biophys.* **1997**, *340*, 239−249.

(6) Whittaker, M. M.; Whittaker, J. W. *J. Biol. Inorg. Chem.* **2002**, *7*, 136−145.

(7) Tanner, A.; Bowater, L.; Fairhurst, S.; Bornemann, S. *J. Biol. Chem.* **2001**, *276*, 43627−43634.

(8) Woo, E.; Dunwell, J.; Goodenough, P.; Marvier, A.; Pickersgill, R. *Nat. Struct. Biol.* **2000**, *7*, 1036−1040.

(9) Dunwell, J. M.; Purvis, A.; Khuri, S. *Phytochemistry* **2004**, *65*, 7−17.

(10) Schwarzenbacher, R. et al. *Proteins* **2004**, *56*, 392−395.

(11) Becke, A. D. J. *Chem. Phys.* **1993**, *98*, 5648−5652.

(12) Lee, C.; Yang, W.; Parr, R. G. *Phys. Rev.* **1988**, *B37*, 785−789.

(13) Frisch, M. J. et al. Gaussian 03, Revision B.03, Gaussian Inc., Pittsburgh, PA, 2003.

(14) Schrödinger, Inc., Portland, Oregon JAGUAR 4.0, 2000.

(15) Tannor, D. J.; Marten, B.; Murphy, R.; Friesner, R. A.; Sitkoff, D.; Nicholls, A.; Ringnalda, M.; Goddard III, W. A.; Honig, B. *J. Am. Chem. Soc.* **1994**, *116*, 11875−11882.

(16) Marten, B.; Kim, K.; Cortis, C.; Friesner, R. A.; Murphy, R.; Ringnalda, M.; Sitkoff, D.; Honig, B. *J. Phys. Chem.* **1996**, *100*, 11775−11788.

(17) Harvey, J. N.; Aschi, M.; Schwarz, H.; Koch, W. *Theor. Chem. Acc.* **1998**, *99*, 95−99.

(18) Schmidt, M. W.; Baldridge, K. K.; Boatz, J. A.; Elbert, S. T.; Gordon, M. S.; Jensen, J. H.; Koseki, S.; Matsunaga, N.; Nguyen, K.; Su, S.; Windus, T. L.; Dupuis, M.; Montgomery, J. A. *J. Comput. Chem.* **1993**, *14*, 1347−1363.

(19) Koseki, S.; Schmidt, M. W.; Gordon, M. S. *J. Phys. Chem.* **1992**, *96*, 10768−10772.

(20) Koseki, S.; Gordon, M. S.; Schmidt, M. W.; Matsunaga, N. *J. Phys. Chem.* **1995**, *99*, 12764−12772.

(21) Nakamura, H. *J. Chem. Phys.* **1987**, *87*, 4031−4041.

(22) Mouesca, J. M.; Chen, J. L.; Noodleman, L.; Bashford, D.; Case, D. A. *J. Am. Chem. Soc.* **1994**, *116*, 11898−11914.

(23) Ciofini, I.; A., D. C. *Coord. Chem. Rev.* **2003**, *238−239*, 187−209.

(24) Siegbahn, P. E. M.; Blomberg, M. R. A. *Chem. Rev.* **2000**, *100*, 421−437.

(25) Blomberg, M. R. A.; Siegbahn, P. E. M. *J. Phys. Chem. B* **2001**, *105*, 9375−9386.

(26) Siegbahn, P. E. M. *Q. Rev. Biophys.* **2003**, *36*, 91−145.

(27) Jensen, K. P.; Ryde, U. *J. Biol. Chem.* **2004**, *279*, 14561−14569.

(28) Lundberg, M.; Siegbahn, P. *Chem. Phys. Lett.* **2005**, *401*, 347−351.

(29) Bassan, A.; Borowski, T.; Siegbahn, P. E. M. *Dalton Trans.* **2004**, *20*, 3153−3162.

(30) Hashimoto, K.; Nagatomo, S.; Fujinami, S.; Furutachi, H.; Ogo, S.; Suzuki, M.; Uehara, A.; Maeda, Y.; Watanabe, Y.; Kitagawa, T. *Angew. Chem.* **2002**, *114*, 1250−1253.

(31) Borowski, T.; Bassan, A.; Siegbahn, P. E. M. *Biochemistry* **2004**, *43*, 12331−12342.

(32) Borowski, T.; Bassan, A.; Siegbahn, P. E. M. *Chem. Eur. J.* **2004**, *10*, 1031−1041.

(33) Borowski, T.; Bassan, A.; Siegbahn, P. E. M. *Inorg. Chem.* **2004**, *43*, 3277−3291.

CT050041R